Photoacoustics 15 (2019) 100143

Contents lists available at ScienceDirect

Photoacoustics

journal homepage: www.elsevier.com/locate/pacs

Optical-resolution photoacoustic microscopy for monitoring vascular normalization during anti-angiogenic therapy

Hui-Chao Zhou[a,b,1], Ningbo Chen[b,c,1], Huangxuan Zhao[b], Tinghui Yin[a], Jianhui Zhang[c], Wei Zheng[b], Liang Song[b], Chengbo Liu[b,**], Rongqin Zheng[a,*]

[a] Department of Medical Ultrasonic, Guangdong Key Laboratory of Liver Disease Research, The Third Affiliated Hospital, Sun Yat-sen University, Guangzhou, China
[b] Research Laboratory for Biomedical Optics and Molecular Imaging, CAS Key Laboratory of Health Informatics, Shenzhen Institutes of Advanced Technology, Chinese Academy of Sciences, Shenzhen, China
[c] School of Mechanical and Electrical Engineering, Guangzhou University, Guangzhou, China

ARTICLE INFO

Keywords:
Optical-resolution photoacoustic microscopy
Tumor
Anti-angiogenesis
Vasculature
Vascular normalization

ABSTRACT

Monitoring the changes in tumor vascularity is important for anti-angiogenic therapy assessment with therapeutic implications. However, monitoring vascularity is quite challenging due to the lack of appropriate imaging techniques. Here, we describe a non-invasive imaging technique using optical-resolution photoacoustic microscopy (OR-PAM) to track vascular changes in prostate cancer treated with an anti-angiogenic agent, DC101, on a mouse ear xenograft model. Approximately 1–3 days after the initial therapy, OR-PAM imaging detected tumor vascular changes such as reduced vessel tortuosity, decreased vessel diameter and homogenized intratumoral vessel distribution. These observations indicated vessel normalization, which was pathologically validated as increased fractional pericyte coverage, functional perfusion and drug delivery of the vessels. After four DC101 interventions, OR-PAM imaging eventually revealed intratumoral vessel regression. Therefore, OR-PAM imaging of the vasculature offers a promising method to study anti-angiogenic drug mechanisms of action in vivo and holds potential in monitoring and guiding anti-angiogenic therapy.

1. Introduction

Tumor angiogenesis can induce excessive vessel growth to render tumor cells more accessible to nutrients, oxygen and metastasis [1]. Therefore, the strategy of anti-angiogenic therapy has been proposed to deprive tumors of their blood supply [2]. The benefit of current anti-angiogenic therapy is far from satisfactory [3], and many efforts have been devoted to identifying new drugs or drug combinations to combat tumor angiogenesis. However, there is still a lack of an effective response evaluation method for anti-angiogenic drug assessment. Imaging of tumor blood perfusion and/or vessel architecture has been demonstrated to help identify cancer patient responders to anti-angiogenic therapy [4,5], suggesting that the changes in the underlying tumor vascular biology are good indicators for assessing anti-angiogenic drug efficacy. Conventional imaging techniques, such as MR, CT, ultrasound or optical imaging, have already been fostered to monitor changes in tumor vascularity resulting from anti-angiogenic therapy [4–7]. However, these techniques cannot resolve fine vasculature and some require exogenous contrast agents. Photoacoustic tomography (PAT) is a newly emerging technique with the potential for imaging vascular morphology, blood oxygenation, and blood flow in vivo at great depth and resolution by using hemoglobin as an endogenous contrast agent [8–13]. There are currently two major implementations of PAT: photoacoustic computed tomography (PACT), which can image vasculature with a larger field of view (FOV), faster speed and deeper depths, and photoacoustic microscopy (PAM), which can visualize vascular networks with higher resolutions, up to ~1-10 μm for optical-resolution PAM (OR-PAM) [12,13]. In this regard, OR-PAM may have an

Abbreviations: OR-PAM, optical-resolution photoacoustic microscopy; PAT, photoacoustic tomography; FBS, fetal bovine serum; α-SMA, α-smooth muscle actin; Dox, doxorubicin; MAP, maximum amplitude projection

* Corresponding author at: Department of Medical Ultrasonic, Guangdong Key Laboratory of Liver Disease Research, The Third Affiliated Hospital, Sun Yat-sen University, Tian He Road 600#, Guangzhou 510630, China.
** Corresponding author at: Research Laboratory for Biomedical Optics and Molecular Imaging, CAS Key Laboratory of Health Informatics, Shenzhen Institutes of Advanced Technology, Chinese Academy of Sciences, 1068 Xueyuan Boulevard, Shenzhen 518055, China.
E-mail addresses: China.cb.liu@siat.ac.cn (C. Liu), zhengrq@mail.sysu.edu.cn (R. Zheng).
[1] These authors contributed equally to this work.

https://doi.org/10.1016/j.pacs.2019.100143
Received 26 March 2019; Received in revised form 17 July 2019; Accepted 9 August 2019
Available online 12 August 2019

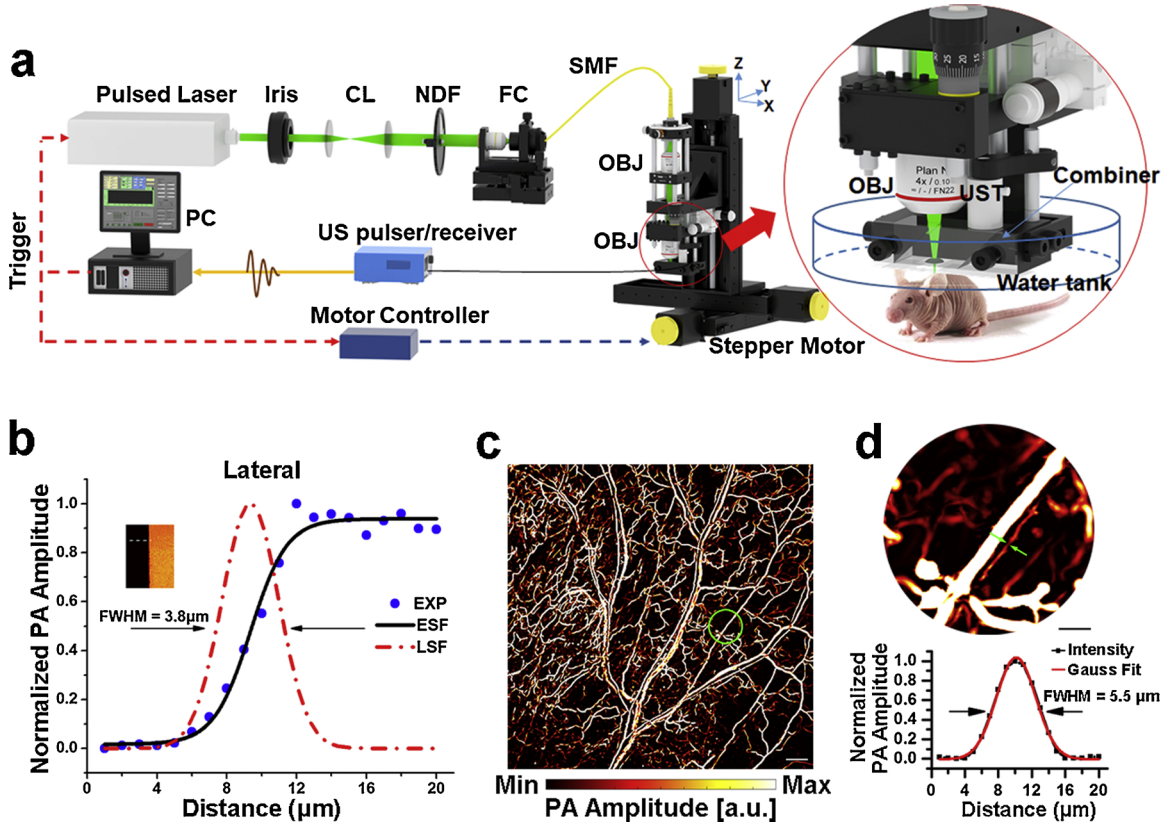

Fig. 1. An overview of the OR-PAM system. (a) The OR-PAM System. CL, convex lens; NDF, neutral density filter; FC, fiber coupler; SMF, single-mode fiber; PC, personal computer. OBJ, objective. UST, ultrasonic transducer. (b) Lateral resolution test on a metallic blade edge. (c) in vivo MAP image of the vascular network from a healthy mouse ear. Scale bar, 0.5 mm. (d) Calibration of the lateral resolution on a blood vessel. The magnified MAP image of the region enclosed by a green circle in (c) is shown at the top of the panel. Scale bar, 100 μm. The cross-sectional PA intensity profile of the blood vessel denoted by green arrows is plotted at the bottom of the panel.

advantage in revealing the subtle alterations of blood vessels, thus allowing early detection of therapeutic response and a better understanding about vascular biology. To date, only one study has employed OR-PAM to evaluate acute vascular destruction due to one-time treatment of vascular-disrupting agents within 5 h [12]. However, many anti-angiogenic drugs induce complicated vascular responses, ranging from vascular normalization to regression [14]. The use of OR-PAM to detect intricate vascular responses and study the course of anti-angiogenic therapy over a longer period has yet to be established.

The importance of tumor angiogenesis imaging is also recognized in optimizing combination therapies. The use of anti-angiogenic drugs in combination with cytotoxic therapy has been shown to yield better survival benefits than monotherapy [15,16]. However, scheduling of this combination therapy should be performed carefully because anti-angiogenic drugs could severely hinder drug delivery by blocking blood supply [17]. This problem can be addressed by the hypothesis of "vascular normalization" [18]: when pro-angiogenic stimulators are counterbalanced by angiogenic inhibitors, the chaotic tumor vasculature can be converted towards a normal state with a relatively regular morphology and improved blood perfusion, resulting in enhanced drug and oxygen delivery [18]. These effects make tumors more sensitive to chemotherapy or radiotherapy, but only for a very limited time [19–21]. The sustained and aggressive uses of anti-angiogenic agents ultimately destroy tumor vasculature. Thus, it is critically important to monitor the normalization time window accurately for scheduling combination therapy. Although OR-PAM is a noninvasive and optimal technology for vascular imaging, whether OR-PAM imaging is useful to track vascular normalization deserves to be investigated.

In this study, we aim to investigate the feasibility of using OR-PAM for longitudinal monitoring of anti-angiogenic therapy and tracking vascular normalization in vivo. A monoclonal antibody against mouse vascular endothelial growth factor receptor-2, DC101, was used in prostate cancer xenografts. To identify the characteristics of tumor vascular responses to DC101, pre- and post-treatment OR-PAM images were acquired, quantitatively analyzed and compared between DC101-treated and control subjects. Histopathological analyses were performed to confirm the functional changes associated with the morphological changes of tumor vessels. Based on these characteristics, we further illustrated the potential of OR-PAM to identify the DC101-induced "normalization window".

2. Materials and methods

2.1. Animal models

Male BALB/c nude mice (4–6 weeks old and weighing 18–20 g) were used in this study. All animal experiments were performed in accordance with the Guide for the Care and Use of Laboratory Animals (National Institutes of Health publication nos. 80-23, revised 1996). The human prostate cancer cell line, C4-2, was cultured in Roswell Park Memorial Institute (RPMI) 1640 medium (Life Technologies, NY, USA) supplemented with 10% fetal bovine serum (FBS; HyClone, UT, USA). The C4-2 cells were suspended in 15 μl PBS and then inoculated into the ears of the mice.

2.2. Experimental design

Twelve tumor-bearing mice were evenly assigned randomly into a

DC101-treated group and a control group. Therapy was initiated on the 6th day after tumor implantation and was designated Day 0. Mice were injected with DC101 (ImClone Systems Inc., NY, USA) intraperitoneally (i.p.) or nonspecific rat IgG at a dose of 40 mg/kg three times on days 0, 2, and 4. On Day 0, prior to the therapy, and on Day 5, each mouse ear with tumor xenografts was imaged to investigate the therapeutic response of the tumor vasculature. After the last imaging, the mice were sacrificed, and the tumor tissues were dissected for histological analysis. To investigate the dynamic vascular changes induced by DC101, another four C4-2 tumor-bearing mice were treated with DC101 and monitored on days 0, 1, 3, 5, and 7. To identify the vascular pattern induced by the prostate cancer tumor, a mouse bearing a C4-2 tumor xenograft without treatment was imaged every 2 days after tumor implantation.

2.3. OR-PAM imaging system and protocol

The custom-built OR-PAM system (Fig. 1a) described in our previous studies [13,22] was used. Briefly, a nanosecond pulsed laser beam at 532 nm from an Nd:YAG laser source (GKNQL-532, Beijing Guoke Laser Co., Beijing, China) was focused for excitation. A repetition rate of 2 kHz was applied in all experiments to obtain A-line signals. The time-resolved photoacoustic signals were detected by a 50-MHz transducer (V214-BC-RM, Olympus-NDT, Japan). The whole scanning head was mounted on a 3-axis motorized translation stage (VT-80, Physik Instrumente, Germany) and controlled by customized computer software written in LabVIEW (2011, National Instruments, TX, USA). To evaluate the lateral resolution of our system, a sharp blade edge was scanned with a step size of 1 μm (inset in Fig. 1b). The measured lateral resolution was ~3.8 μm by deriving the line spread function (LSF) and calculating the full-width at half-maximum (FWHM) of the LSF (Fig. 1b). As shown in Fig. 1c, this resolution is sufficient to evaluate intricate microvasculature. Capillaries as small as 5.5 μm can be resolved in these OR-PAM images (Fig. 1d).

After anesthetization with a mixture of isoflurane (Euthanex, Palmer, Pennsylvania, USA) and air, the mouse ear was flattened on a plastic plate. The scanning was performed at a 5 μm step size between adjacent B-scans. For scanning an $8 \times 8\ mm^2$ region of interest with an 8 mm/s mechanical axis scanning speed, the total imaging time is approximately 30 min, and the B-scan rate is 1 Hz. In all in vivo imaging experiments, the laser energy reaching the tissue surface was maintained at ~200 nJ/pulse, corresponding to an optical fluence of ~16 mJ/cm^2 (when focused ~250 μm beneath the skin surface), which is within the laser safety limit of the American National Standards Institute [Laser Institute of America, American National Standard for Safe Use of Lasers ANSI Z136. New York, NY: American National Standards Institute Inc; 2007].

2.4. Histological analysis

To evaluate the coverage of pericytes on tumor vessels, double immunofluorescence of CD31 (rat antibody against mouse CD31, BD Pharmingen, CA, USA) and α-smooth muscle actin (α-SMA, rabbit polyclonal antibody against mouse α-SMA, Abcam, Cambridge, UK) was performed on tumor tissue sections. The tissue sections were examined using a confocal microscope (Leica, Hamburg, Germany), and images were taken to quantify areas positive for CD31 or α-SMA using ImageJ software (http://rsb.info.nih.gov/ij).

Tumor perfusion was assessed by intravenously injecting 0.05 mg lectin-FITC (Lycopersicon esculentum; Vector Laboratories, CA, USA) 15 min before the mice were sacrificed. To validate the vascular distribution imaged by OR-PAM, the whole tumor section was scanned by a confocal microscope (Leica). To determine the perfusion of vessels, immunofluorescent staining for CD31 was performed on the tumor sections, which were then examined under the confocal microscope (Leica). Images were recorded to calculate the lectin-positive areas relative to the CD31-positive areas.

To evaluate the vascular function of drug delivery, we administered the red autofluorescent chemotherapeutic agent doxorubicin (Dox, 20 mg/kg body weight) intravenously 5 days after the initial DC101 or IgG treatment. Three hours after Dox injection, mice received 0.05 mg lectin-FITC intravenously 15 min before the mice were sacrificed. The distribution of Dox- and lectin-labeled vessels was imaged using a confocal microscope (Leica) to quantify the Dox signal.

2.5. Statistical analysis

Image processing and vascular quantification were analyzed using our developed algorithm implemented in MATLAB (R2014a, The Mathworks, Natick, MA, USA) as previously described [22]. Briefly, the raw 3-D volume data were processed with a Hessian matrix-based algorithm to generate maximum amplitude projection (MAP) images for photoacoustic imaging. The vascular walls were extracted from the original 3-D volume data by background noise degradation, vascular signal identification, vascular signal enhancement, and extraction region growth. Then, the binary volume data were separated into individual subdomains so that no connected components (i.e., connected vessels) existed in each subdomain. An augmented fast marching method (AFMM) was applied in each subdomain to identify the vascular centerlines. Based on the identified centerlines, vessel diameter, density, and tortuosity were computed to describe the properties of the vascular morphology. Vessel diameter was determined by measuring the vertical distances between the centerline and both sides of the vessel walls. The vessel density was represented as the ratio of all vessel pixels to the overall pixels of the selected tumor regions. The vessel tortuosity was assessed by calculating the ratio between the actual path length of a vessel segment in each subdomain and the linear distance between the two ends of the vessel.

Data are presented as the mean ± standard error of the mean (SEM). The differences between pre- and post-treatment were determined by a two-sample Student's t-test. The differences between the control and DC101-treated groups were analyzed using an unpaired Student's t-test. A P-value ≤ 0.05 was considered statistically significant for all comparisons. Analyses were performed with GraphPad Prism (version 5, GraphPad Software, Inc., CA, USA).

3. Results

3.1. Longitudinal imaging of vasculature development within prostate tumor xenografts

We first applied the OR-PAM system at a wavelength of 532 nm to image the development of prostate tumor vasculature based on the endogenous contrast of hemoglobin. A mouse bearing the C4-2 tumor xenograft was selected and imaged every other day from Day 2 to Day 10 following inoculation of tumor cells. As shown in Fig. 2a, the PAM images of the tumor mass showed vessels of varying diameters and revealed an irregular and chaotic vascular network, which was clearly distinguishable compared to the well-established vasculature in the normal tissues. The tumor vessels were heterogeneously distributed throughout the tumor, with a dense network at the tumor periphery compared to the tumor center. As the tumor grew, the tumor center became progressively hypovascular. Moreover, the structural (vessel diameter and density) and geometrical parameters (tortuosity) were quantified to evaluate tumor angiogenesis. All vascular parameters gradually increased (Fig. 2b), consistent with the characteristics of tumor vascular development [1].

3.2. Detecting vascular normalization within prostate tumor xenografts with OR-PAM imaging

To investigate the potential of OR-PAM to detect the tumor

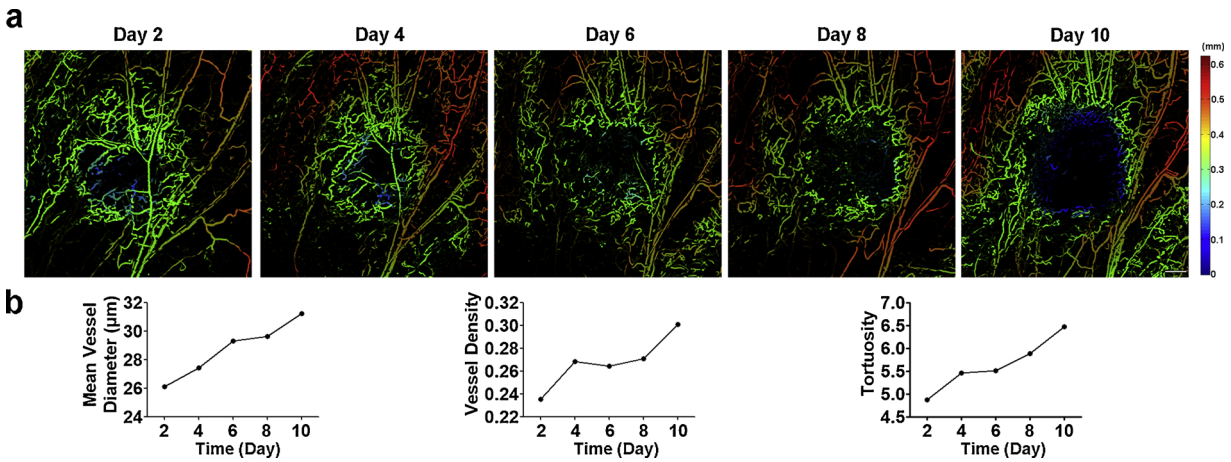

Fig. 2. Longitudinal imaging of developing C4-2 tumor vascular network. (a) The depth-encoded MAP of tumor vascularity. Scale bar, 0.5 mm. (b) Quantification of tumor vasculature. The vasculature within the prostate tumor was imaged on Day 2, Day 4, Day 6, Day 8, and Day 10 following inoculation of C4-2 cells.

therapeutic response, we imaged the tumor vasculature before and 5 days after the initial therapy. The vascular changes in the prostate tumors induced by IgG and DC101 treatment were compared. Consistent with tumors without treatment, as shown in Fig. 2a, the IgG-treated tumors remained highly vascularized in the tumor periphery and less vascularized in the tumor center (Fig. 3a, upper panel). In contrast, the central regions of tumors treated with DC101 were more perfused after treatment since more intratumoral vessels existed (Fig. 3a, lower panel). After the final imaging, mice were injected with lectin to label the vessels. Tumors were then excised and subjected to histological examination. Lectin staining for the control group was sparse in the tumor center but evenly distributed throughout the DC101-treated tumors, confirming the differences in spatial vascular distribution revealed by OR-PAM imaging (Fig. 3b).

To gain quantitative insight into tumor vessel morphologies, the vascular parameters (diameter, density and tortuosity) were obtained from IgG- and DC101-treated tumors before and after treatment (Fig. 3c). In the control group, a significant increase was observed in vessel diameters (29.81 ± 1.39 μm vs. 31.87 ± 0.81 μm, $P = 0.042$), density (0.26 ± 0.03 vs. 0.32 ± 0.03, $P = 0.029$) and tortuosity (5.82 ± 0.30 vs. 6.69 ± 0.24, $P = 0.047$), confirming the increasing abnormal changes of tumor vessels. In the DC101-treated group, vessel diameter dramatically decreased from 28.78 ± 0.99 μm to 26.92 ± 0.70 μm following treatment ($P = 0.015$). The vessel density appeared to remain unaffected by treatment (0.26 ± 0.02 to 0.21 ± 0.02, $P = 0.26$). The mean tortuosity after DC101 treatment was dramatically lower than that of the pretreatment (5.82 ± 0.29 vs. 5.02 ± 0.23, $P = 0.02$). Together with the homogenizing vascular distribution, the decreases in vessel diameter and tortuosity indicate that the tumor vessels were morphologically normalized after DC101 treatment.

To gain the functional information associated with morphologic changes of tumor vasculature, histological analyses were performed. Since the recruitment of pericytes by nascent blood vessels is necessary for vessel maturation and function [23], we first assessed the association of pericytes with tumor vessels by determining the expression of α-SMA, a marker for pericytes. Tumor vessels in IgG-treated control tumors were largely immature with poor pericyte coverage. In comparison, DC101 relatively normalized the wall structures of residual tumor vessels. The fractional coverage of tumor vessels by α-SMA-positive cells in DC101-treated tumors increased from 50.03 ± 6.45% to 68.19 ± 4.11% ($P = 0.039$, Fig. 4a). Vascular perfusion was examined by injecting lectin-FITC intravenously. Approximately 53.81% of the vessels within the control tumors had little or no perfusion. On the other hand, DC101 treatment relieved the intratumor ischemic condition by significantly increasing the percentage of perfused blood vessels (control vs. DC101, 46.19 ± 3.86% vs. 67.35 ± 2.66%, $P = 0.001$, Fig. 4b). We also studied the effect of DC101 on the delivery of a chemotherapeutic agent, doxorubicin (Dox). In the control group, Dox was observed predominantly in proximity to the blood vessels, whereas in the DC101-treated tumors, the fluorescent signal generated from Dox displayed a significant increase of distribution within tumors (Fig. 4c). Quantitative analysis confirmed the increase of Dox uptake following pretreatment with DC101 (control vs. DC101, 20.24 ± 1.64% vs. 33.20 ± 2.47%, $P = 0.001$, Fig. 4c).

Collectively, the vascular morphologic normalization observed by OR-PAM can be related to functional normalization. By observing vascular distribution and measuring vessel diameter and tortuosity, OR-PAM can detect vascular normalization.

3.3. Serial PA imaging of tumor vasculature to define the course of DC101 treatment

Although DC101 treatment transforms tumor vasculature into a relatively normal state, the normalization window is always assumed to be short-lived and would close with an onset of vascular regression, which would compromise drug delivery [18–21]. Thus, the course of therapy should be carefully monitored for scheduling combined therapies. Herein, we also tested OR-PAM for tracking the dynamic therapeutic responses of tumor-bearing mice receiving DC101 treatment. The serial observation is shown in Fig. 5. A gradual normalization of vascular morphology was noted from Day 1 to Day 5 following DC101 administration. Consistent with previous results, treatment with DC101 resulted in a more homogenous distribution of perfusion and a less chaotic vascular network within the tumor xenografts. However, prolonged DC101 treatment eventually pruned away the normalized intratumoral vessels with a more visible difference in vessel distribution between the tumor center and the tumor periphery on Day 7, which potentially indicated the start of closing the optimal time window for synergistic cytotoxic therapy.

4. Discussion and conclusion

Imaging of tumor vasculature with high resolution, which enables us to measure temporal and spatial vascular changes with therapeutic implications, is of great importance. In this study, we presented an OR-PAM system capable of resolving blood vessels down to 5.5 μm as a promising solution for longitudinal monitoring of vascular responses to anti-angiogenic tumor therapy by evaluating the DC101 effect on prostate cancer tumors. Based on the phenotypic morphological

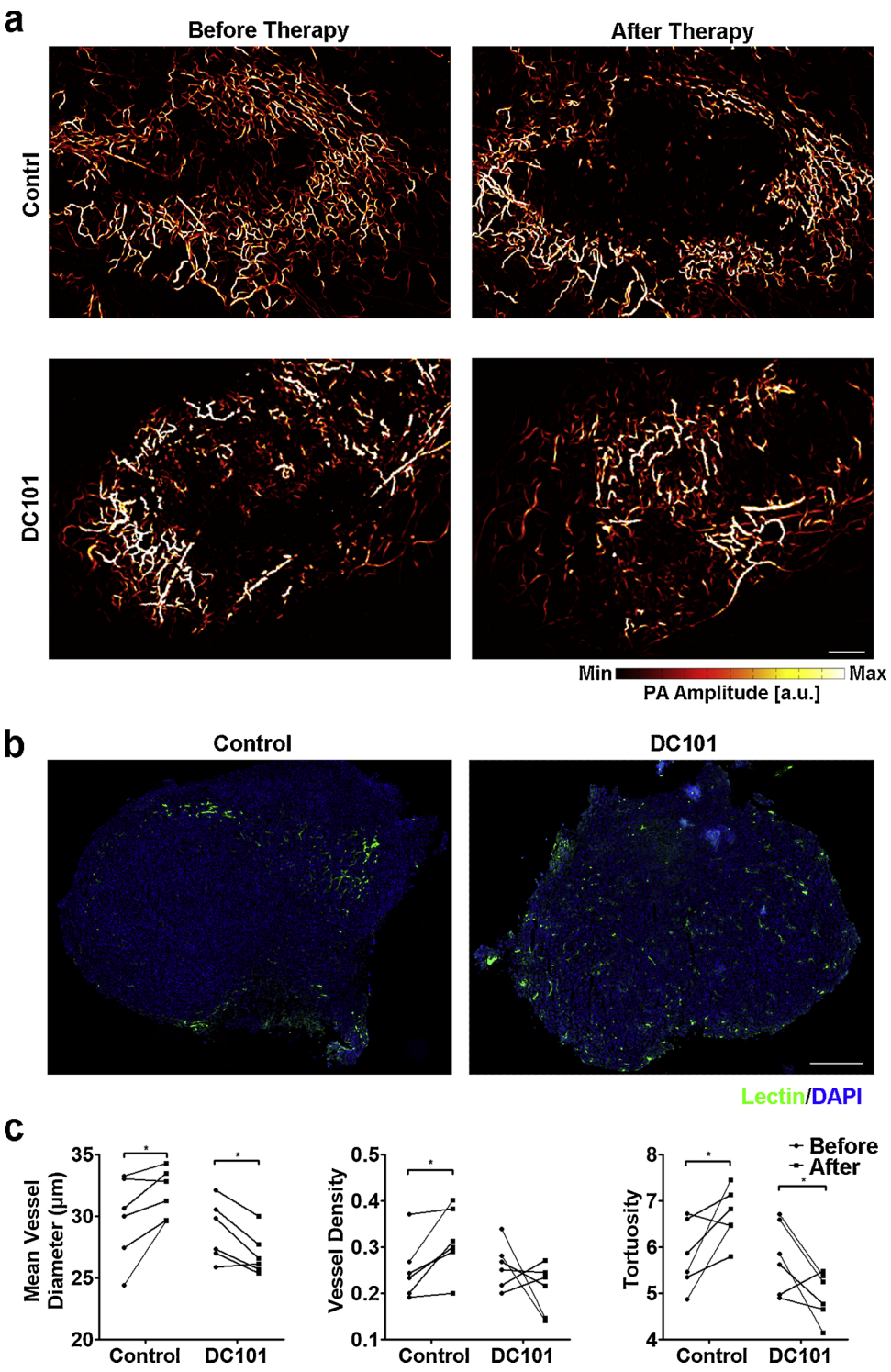

Fig. 3. OR-PAM characterized the vascular responses to DC101 therapy. (a) Representative images of MAP focused on control and DC101-treated tumors before or 5 days after the initial treatment. Each mouse received the indicated therapy three times at two-day intervals. Scale bar, 0.5 mm. (b) Histological examination of the vascular spatial distribution within the tumors treated with control antibody or DC101. Fluorescence-labeled lectin (green) outlined the tumor vessels. Nuclei were counterstained blue with DAPI. Scale bar, 0.5 mm. (c) Multiparametric quantitative analysis of tumor vasculature in different groups. Control (IgG), n = 6; DC101, n = 6. *, $P < 0.05$.

changes of the vasculature, OR-PAM imaging was able to detect vascular normalization and regression in vivo over the course of DC101 treatment.

To date, the feasibility of PAM in monitoring anti-angiogenic therapy in a murine tumor xenograft model has been shown by one previous study [12], which performed imaging on tumors that were too small to clearly visualize the intratumoral vessels. They evaluated acute drug effects mainly based on the intensity of the photoacoustic signal. In our study, we took full advantage of OR-PAM to resolve tumor vasculature and measure more parameters: vessel diameter, density and tortuosity. These three parameters are commonly used for evaluating anti-angiogenic therapy [7,19]. The degree of tumor vessel density has long been considered an indicator of tumor angiogenic activity. Vessel diameter and tortuosity are important parameters of vascular morphology. Tumor vessel diameter, at some point, is associated with vessel maturation because it can be increased by loss of pericyte coverage or loosened endothelium-pericyte interaction [24,25]. Tortuosity not only describes the irregular shape of tumor vessels but is also presumed to be associated with blood flow. A decreased tortuosity can be beneficial by shortening blood flow pathways [26]. By incorporating

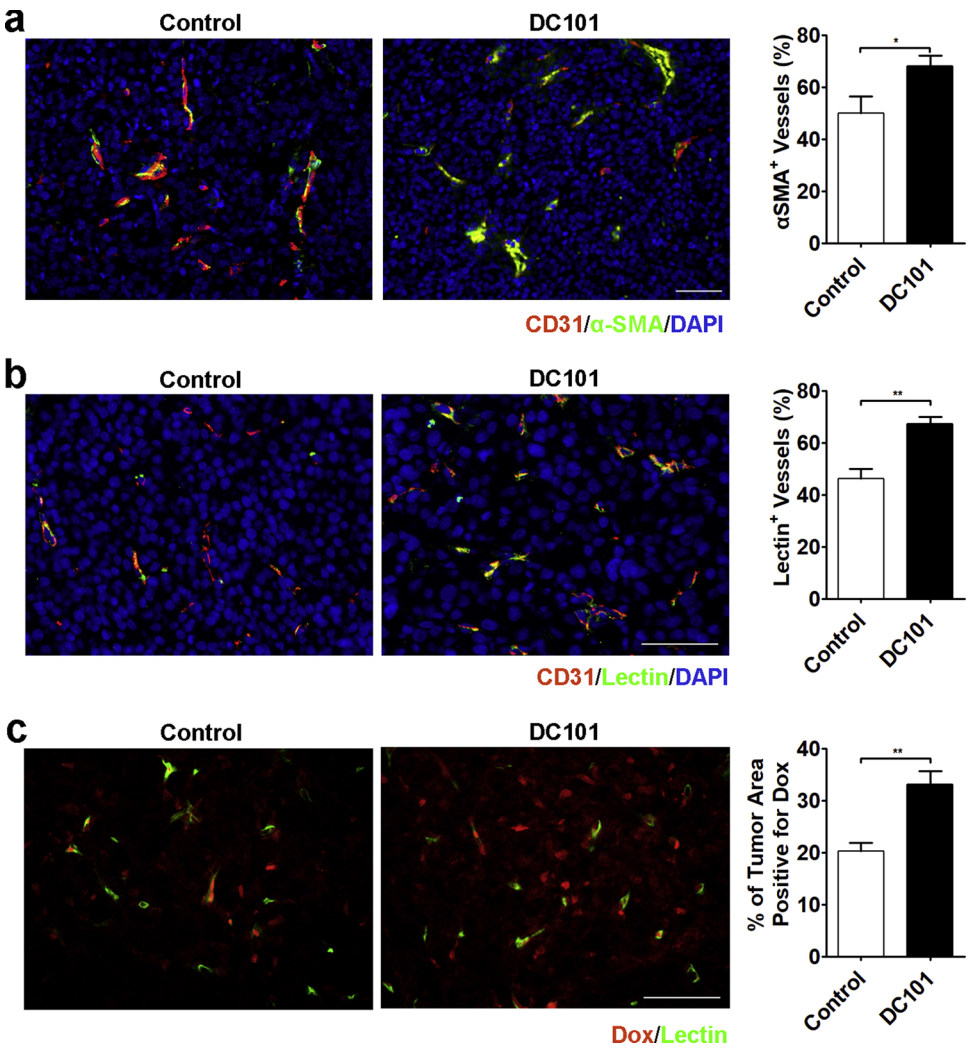

Fig. 4. Histological analysis confirmed the normalization of vascular functions after DC101 treatment. (a) Representative images and quantification of pericyte coverage by immunofluorescent double staining for endothelial cells (CD31) and pericytes (α-SMA) in the sections of control and DC101-treated tumors. (b) Representative images and quantification of perfused blood vessels (lectin-FITC) and immunofluorescence staining for endothelial cells (CD31) in the sections of control and DC101-treated tumors. (c) Representative images and quantification of intratumoral doxorubicin distribution in the sections of control and DC101-treated tumors. Fluorescence-labeled lectin (green) outlines the tumor vessels. Nuclei were counterstained blue with DAPI. Scale bar, 50 μm. *, $P < 0.05$; **, $P < 0.01$.

multiple quantitative parameters, OR-PAM images provided more insight into the therapeutic response in addition to vascular disruption, as we presented in the results section.

While vascular disruption can be visualized as a reduction of photoacoustic intensity, the ability of PAM to detect vascular normalization has not been studied. To address this issue, we compared the observed vascular changes between tumors with DC101 and control therapy to identify OR-PAM imaging indicators of the normality of tumor vascular physiology. The OR-PAM images showed a vascular rim pattern for prostate tumors at different time points during their development. After drug administration, the DC101-treated tumors showed improved blood support in their central regions, while the control tumors still displayed a central ischemic character. This observed difference was validated by histological examination of lectin staining. Moreover, quantitative morphologic analysis revealed significantly decreased vessel diameter and tortuosity in DC101-treated tumors compared with control tumors. These pronounced morphological changes coincided with functional normalization, as evidenced by the significant increase in the pericyte coverage of tumor vessels, vascular perfusion, and drug delivery. Therefore, the vascular distribution pattern visible in OR-PAM images and the morphologic parameters (vessel diameter and tortuosity) derived therefrom can potentially serve as imaging biomarkers to predict vascular normalization.

Currently, the concept of “normalizing tumor vasculature” [18] is widely accepted in explaining the synergistic anti-tumor effect and scheduling anti-angiogenic therapy with chemotherapy. However, it is challenging to define the timing of the normalization window wherein cytotoxic drugs will have maximal access to cancer cells during the treatment intervention. Based on the above-described OR-PAM imaging parameters, our study observed an early onset of normalization, approximately 1–3 days after the commencement of initial therapy, which was consistent with previous studies [7,19,20]. The closure of the normalization window has been proposed to be related to prolonged dosing of anti-angiogenic therapies, which would tip the balance past the equilibrium in favor of anti-angiogenic molecules and subsequently lead to vascular pruning/regression [21]. As OR-PAM resolves vasculature through hemoglobin absorption, the reduced intratumoral vascularization observed by OR-PAM could somehow reflect the decrease of efficient pathways for delivering drugs into solid tumors. Therefore, we postulated that the normalization window may begin to close at the occurrence of the regression of normalized intratumoral vessels. In this study, we successfully observed dynamic vascular changes from normalization to regression using OR-PAM imaging. These results suggest that OR-PAM can be very helpful to identify the normalization window in vivo, thus providing information about the optimal timing to administrate chemotherapy drugs.

Preclinical drug assessments in small animal cancer models are very important in guiding us to choose drug candidates and design therapeutic strategies. In this study, we evaluated a subcutaneous ear implantation model, which is easy to image and can avoid unnecessary motion artifacts. Although this model is considered a less accurate recapitulation of cancers than an orthotopic model, it still breeds tumors

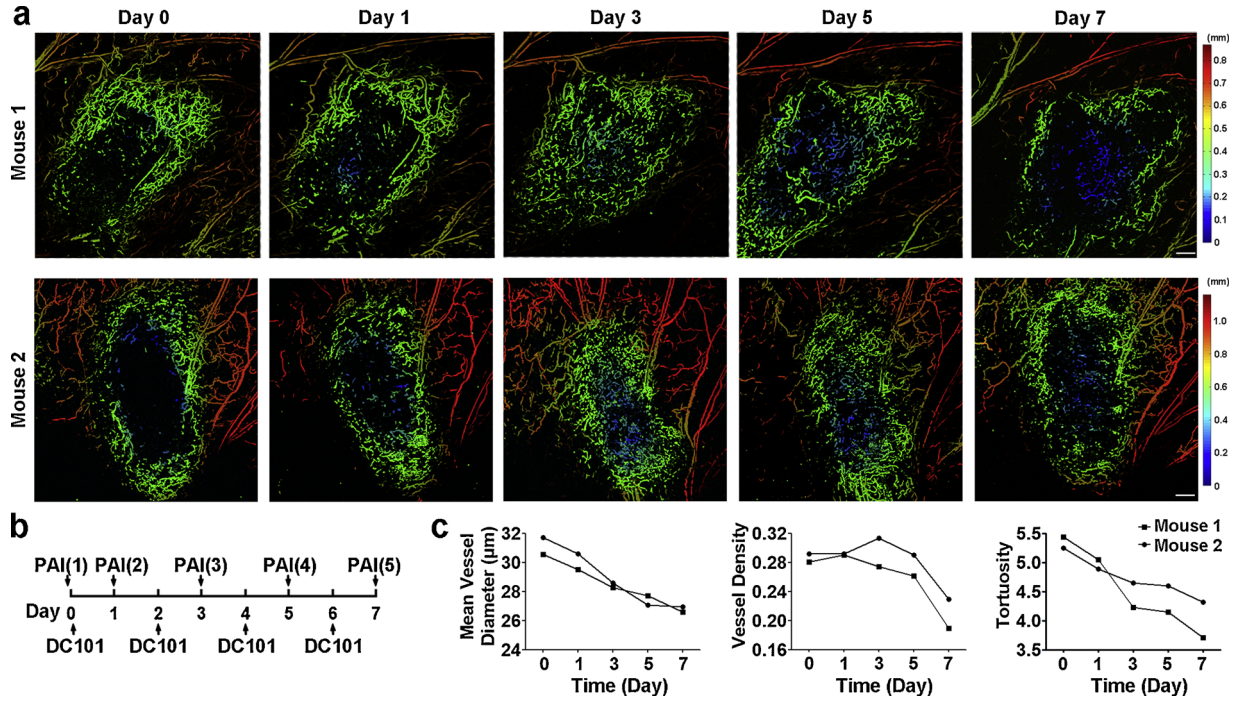

Fig. 5. OR-PAM monitored the dynamic changes of tumor vasculature in response to DC101 therapy. (a) The depth-encoded MAP of tumor vascularity. Scale bar, 0.5 mm. (b) Schematic of therapy response monitoring. The vasculature within the prostate tumors was imaged on Day 0 before treatment and on Day 1, Day 3, Day 5, and Day 7 after the initial therapy. (c) Quantification of tumor vasculature.

that display similar vascular characteristics to those growing on orthotopic sites [7,27] and is applied in many other preclinical angiogenesis studies [28,29]. Applying OR-PAM in this model provides a convenient intravital tumor imaging method that helps us preliminarily screen vascular-targeting drugs or molecules and understand their specific effect on vasculature over time. Based on the relationship between visible features and vascular function, we can be informed of whether and in which type of cancer a drug/molecule can induce vascular normalization and how long they remain in that state, consequently informing the decision in choosing the most optimal anti-angiogenic drug/target to enhance chemotherapy. It is also worthwhile to note that portable OR-PAM has been developed [30,31], which may increase the clinical feasibility of OR-PAM to evaluate angiogenesis in superficial tumors of patients.

The current study, while demonstrating several advantages of OR-PAM, has a few limitations. Our system was implemented with a single wavelength laser source specific to hemoglobin. Thus, we could only observe the absorbance of total hemoglobin. By extending the system to use multiple wavelengths, oxy- and deoxyhemoglobin information can also be visualized, which would provide additional information on vascular function. Another limitation of our study is the number of animals used for serial monitoring during the DC101 treatment. The manifestation of vessel regression after normalization within 7 days was only observed in two mice out of the four used. This might be attributed to individual differences that caused different durations of normalization windows, which supports the necessity of continuous monitoring for individual therapy.

In conclusion, our study provides proof to support the applicability of OR-PAM for noninvasive assessment of the anti-angiogenic drug therapy response over time in preclinical mouse models. The vascular characteristics acquired by OR-PAM imaging can inform both vascular normalization and regression by illuminating the time window of normalization. This imaging technique can be widely used in the screening and development of vascular targeted drugs and holds great potential in the optimal designing of anti-angiogenic therapy with chemotherapy.

Funding

This work was supported by grants from National Natural Science Foundation of China [81430038, 81602151, 91739117, 81601512, 81522024, 81427804, 81672438]; from National Key Basic Research (973) Program of China grant [2015CB755500]; from Guangdong Natural Science Foundation grant [2014A030312006]; from Science and Technology Planning Project of Guangdong Province [2017A020215131]; from Shenzhen Science and Technology Innovation [JCYJ20170413153129570]; from Guangzhou Science and Technology Innovation grant [201604020144] and Chinese Academy of Sciences grant [GJJSTD20180002, SKLA-2018-03].

Declaration of Competing Interest

The authors declare that there are no conflicts of interest.

Acknowledgment

We would like to thank Professor Rakesh K. Jain and Professor Bronislaw Pytowski for kindly providing DC101.

References

[1] D. Hanahan, R.A. Weinberg, Hallmarks of cancer: the next generation, Cell 5 (144) (2011) 646–674, https://doi.org/10.1016/j.cell.2011.02.013.
[2] J. Folkman, Tumor angiogenesis: therapeutic implications, N. Engl. J. Med. 21 (285) (1971) 1182–1186, https://doi.org/10.1056/NEJM197111182852108.
[3] J.N. Bottsford-Miller, R.L. Coleman, A.K. Sood, Resistance and escape from anti-angiogenesis therapy: clinical implications and future strategies, J. Clin. Oncol. 32 (30) (2012) 4026–4034, https://doi.org/10.1200/JCO.2012.41.9242.
[4] A.G. Sorensen, K.E. Emblem, P. Polaskova, et al., Increased survival of glioblastoma patients who respond to antiangiogenic therapy with elevated blood perfusion, Cancer Res. 2 (72) (2012) 402–407, https://doi.org/10.1158/0008-5472.CAN-11-2464.
[5] K.E. Emblem, K. Mouridsen, A. Bjornerud, et al., Vessel architectural imaging identifies cancer patient responders to anti-angiogenic therapy, Nat. Med. 9 (19) (2013) 1178–1183, https://doi.org/10.1038/nm.3289.

[6] D. Sampath, J. Oeh, S.K. Wyatt, et al., Multimodal microvascular imaging reveals that selective inhibition of class I PI3K is sufficient to induce an antivascular response, Neoplasia 7 (15) (2013) 694–711.
[7] B.J. Vakoc, R.M. Lanning, J.A. Tyrrell, et al., Three-dimensional microscopy of the tumor microenvironment in vivo using optical frequency domain imaging, Nat. Med. 10 (15) (2009) 1219–1223, https://doi.org/10.1038/nm.1971.
[8] L.V. Wang, S. Hu, Photoacoustic tomography: in vivo imaging from organelles to organs, Science 6075 (335) (2012) 1458–1462, https://doi.org/10.1126/science.1216210.
[9] S.E. Bohndiek, L.S. Sasportas, S. Machtaler, et al., Photoacoustic tomography detects early vessel regression and normalization during ovarian tumor response to the antiangiogenic therapy trebananib, J. Nucl. Med. 12 (56) (2015) 1942–1947, https://doi.org/10.2967/jnumed.115.160002.
[10] A. Chekkoury, A. Nunes, J. Gateau, et al., High-resolution multispectral optoacoustic tomography of the vascularization and constitutive hypoxemia of cancerous tumors, Neoplasia 8 (18) (2016) 459–467, https://doi.org/10.1016/j.neo.2016.06.004.
[11] A. Orlova, M. Sirotkina, E. Smolina, et al., Raster-scan optoacoustic angiography of blood vessel development in colon cancer models, Photoacoustics (13) (2019) 25–32, https://doi.org/10.1016/j.pacs.2018.11.005.
[12] R. Bi, G. Balasundaram, S. Jeon, et al., Photoacoustic microscopy for evaluating combretastatin A4 phosphate induced vascular disruption in orthotopic glioma, J. Biophotonics 10 (11) (2018) e201700327, , https://doi.org/10.1002/jbio.201700327.
[13] R. Lin, J. Chen, H. Wang, et al., Longitudinal label-free optical-resolution photoacoustic microscopy of tumor angiogenesis in vivo, Quant. Imaging Med. Surg. 1 (5) (2015) 23–29, https://doi.org/10.3978/j.issn.2223-4292.2014.11.08.
[14] S. Tugues, S. Koch, L. Gualandi, X. Li, L. Claesson-Welsh, Vascular endothelial growth factors and receptors: anti-angiogenic therapy in the treatment of cancer, Mol. Aspects Med. 2 (32) (2011) 88–111, https://doi.org/10.1016/j.mam.2011.04.004.
[15] H.D. Bear, G. Tang, P. Rastogi, et al., Bevacizumab added to neoadjuvant chemotherapy for breast cancer, N. Engl. J. Med. 4 (366) (2012) 310–320, https://doi.org/10.1056/NEJMoa1111097.
[16] N.Y. Lee, Q. Zhang, D.G. Pfister, et al., Addition of bevacizumab to standard chemoradiation for locoregionally advanced nasopharyngeal carcinoma (RTOG 0615): a phase 2 multi-institutional trial, Lancet Oncol. 2 (13) (2012) 172–180, https://doi.org/10.1016/S1470-2045(11)70303-5.
[17] A.A. Van der Veldt, M. Lubberink, I. Bahce, et al., Rapid decrease in delivery of chemotherapy to tumors after anti-VEGF therapy: implications for scheduling of anti-angiogenic drugs, Cancer Cell 1 (21) (2012) 82–91, https://doi.org/10.1016/j.ccr.2011.11.023.
[18] R.K. Jain, Normalization of tumor vasculature: an emerging concept in antiangiogenic therapy, Science 5706 (307) (2005) 58–62, https://doi.org/10.1126/science.1104819.
[19] F. Winkler, S.V. Kozin, R.T. Tong, et al., Kinetics of vascular normalization by VEGFR2 blockade governs brain tumor response to radiation: role of oxygenation, angiopoietin-1, and matrix metalloproteinases, Cancer Cell 6 (6) (2004) 553–563, https://doi.org/10.1016/j.ccr.2004.10.011.
[20] P.V. Dickson, J.B. Hamner, T.L. Sims, et al., Bevacizumab-induced transient remodeling of the vasculature in neuroblastoma xenografts results in improved delivery and efficacy of systemically administered chemotherapy, Clin. Cancer Res. 13 (13) (2007) 3942–3950, https://doi.org/10.1158/1078-0432.CCR-07-0278.
[21] S. Goel, D.G. Duda, L. Xu, et al., Normalization of the vasculature for treatment of cancer and other diseases, Physiol. Rev. 3 (91) (2011) 1071–1121, https://doi.org/10.1152/physrev.00038.2010.
[22] H. Zhao, G. Wang, R. Lin, et al., Three-dimensional Hessian matrix-based quantitative vascular imaging of rat iris with optical-resolution photoacoustic microscopy in vivo, J. Biomed. Opt. 4 (23) (2018) 1–11, https://doi.org/10.1117/1.JBO.23.4.046006.
[23] R.K. Jain, Molecular regulation of vessel maturation, Nat. Med. 6 (9) (2003) 685–693, https://doi.org/10.1038/nm0603-685.
[24] S. Morikawa, P. Baluk, T. Kaidoh, et al., Abnormalities in pericytes on blood vessels and endothelial sprouts in tumors, Am. J. Pathol. 3 (160) (2002) 985–1000, https://doi.org/10.1016/S0002-9440(10)64920-6.
[25] P. Nasarre, M. Thomas, K. Kruse, et al., Host-derived angiopoietin-2 affects early stages of tumor development and vessel maturation but is dispensable for later stages of tumor growth, Cancer Res. 4 (69) (2009) 1324–1333, https://doi.org/10.1158/0008-5472.CAN-08-3030.
[26] J.W. Baish, T. Stylianopoulos, R.M. Lanning, et al., Scaling rules for diffusive drug delivery in tumor and normal tissues, Proc. Natl. Acad. Sci. U. S. A. 5 (108) (2011) 1799–1803, https://doi.org/10.1073/pnas.1018154108.
[27] T. Poschinger, A. Renner, F. Eisa, et al., Dynamic contrast-enhanced micro-computed tomography correlates with 3-dimensional fluorescence ultramicroscopy in antiangiogenic therapy of breast cancer xenografts, Invest. Radiol. 7 (49) (2014) 445–456, https://doi.org/10.1097/RLI.0000000000000038.
[28] J. Yao, K.I. Maslov, Y. Zhang, Y. Xia, L.V. Wang, Label-free oxygen-metabolic photoacoustic microscopy in vivo, J. Biomed. Opt. 7 (16) (2011) 76003, https://doi.org/10.1117/1.3594786.
[29] S.S. Oladipupo, S. Hu, A.C. Santeford, et al., Conditional HIF-1 induction produces multistage neovascularization with stage-specific sensitivity to VEGFR inhibitors and myeloid cell independence, Blood 15 (117) (2011) 4142–4153, https://doi.org/10.1182/blood-2010-09-307538.
[30] K. Park, J.Y. Kim, C. Lee, et al., Handheld photoacoustic microscopy probe, Sci. Rep. 1 (7) (2017) 13359, https://doi.org/10.1038/s41598-017-13224-3.
[31] Q. Chen, H. Guo, T. Jin, et al., Ultracompact high-resolution photoacoustic microscopy, Opt. Lett. 7 (43) (2018) 1615–1618, https://doi.org/10.1364/OL.43.001615.

Hui-Chao Zhou is a research assistant of Department of Medical Ultrasonic at the Third Affiliated Hospital of Sun Yat-sen University. She received her Ph.D degree from Sun Yat-sen University. Her research focuses on the molecular medicine and molecular imaging.

Ningbo Chen is currently pursuing his Master's degree in the School of Mechanical and Electrical Engineering at Guangzhou University in China. His research interests include developing novel biomedical imaging tools based on photoacoustic imaging for preclinical and clinical applications.

Huangxuan Zhao received his bachelor's degree in mechanical engineering from Wuhan University of Technology in 2013. Currently, he is pursuing his PhD degree in the Department of Biomedical Engineering at Capital Medical University in China. His research interests include utilizing photoacoustic imaging for the detection of diseases and developing new surgical guidance methods for clinical applications.

Tinghui Yin is an attending doctor at the Department of Medical Ultrasonic, The Third Affiliated Hospital of Sun Yat-sen University. His research focuses on the clinical and pre-clinical applications of multi-modality molecular imaging, especially on molecular ultrasound and photoacoustic imaging technologies.

Jianhui Zhang is currently a professor and a PhD candidate supervisor at Guangzhou University, China. His research interests include mechanical design and its theory, piezoelectric driving, and photoacoustic tomography.

Wei Zheng is a professor at SIAT, CAS. He received his B.S. degree in Optical Engineering from Zhejiang University in 2003, his Ph.D. degree in Electronic and Computer Engineering from Hong Kong University of Science and Technology in 2011. His research focuses on biomedical optics, including fluorescence spectroscopy, fluorescence microscopy and nonlinear optical microscopy.

Liang Song is a professor at SIAT, CAS and founding directors of The Research Lab for Biomedical Optics, and The Shenzhen Key Lab for Molecular Imaging. Prior to joining SIAT, he studied at Washington University, St. Louis and received his Ph.D. in Biomedical Engineering. His research focuses on multiple novel photoacoustic imaging technologies.

Chengbo Liu is an Associate Professor at SIAT, CAS. He received both his Ph.D and Bachelor degree from Xi'an Jiaotong University, each in 2012 in Biophysics and 2007 in Biomedical Engineering. During his Ph.D. training, he spent two years doing tissue spectroscopy research at Duke University as a visiting scholar. Now he is an associate professor at SIAT, working on multi-scale photoacoustic imaging and its translational research.

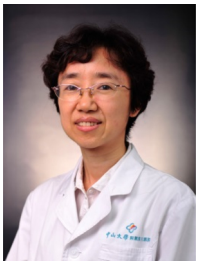

Rongqin Zheng is a professor and a PhD candidate supervisor at the Department of Medical Ultrasonic, The Third Affiliated Hospital of Sun Yat-sen University. Her research focuses on the clinical and pre-clinical applications of novel imaging technologies, including molecular ultrasound imaging and photoacoustic imaging.